

# Density functional theory study on the adsorption of H, OH, and CO and coadsorption of CO with H/OH on the Pt<sub>2</sub>Ru<sub>3</sub> surfaces

Md. Khorshed Alam, Shuhei Saito, and Hiromitsu Takaba<sup>a)</sup>

*Department of Environmental Chemistry and Chemical Engineering, School of Advanced Engineering, Kogakuin University, Hachioji, Tokyo 192-0015, Japan*

(Received 19 April 2016; accepted 22 July 2016)

This paper presents a periodic density functional theory study on the adsorption of H, CO, and OH on Pt<sub>2</sub>Ru<sub>3</sub> alloy surfaces containing different conformations of Pt and Ru atoms. The results show that for separate adsorption, H is preferentially adsorbed at Pt sites, whereas CO and OH are preferentially adsorbed at Ru sites. The adsorption strengths of H, CO, and OH are affected by ratio of the alloying atoms in top surface, the nature of the neighboring atom nearest to the adsorption site, and the conformation of alloying atoms in subsurface. We also investigated the coadsorption of CO with OH and the coadsorption of CO with H and found that the Pt–CO bond strength weakens. We also uncovered some information about the competitive adsorption behavior of adsorbates (CO, OH) with the aim of designing CO-tolerant Pt–Ru alloy catalysts.

## I. INTRODUCTION

The adsorption and oxidation of CO on metal electrodes fundamental problems in heterogeneous catalysis, electrochemistry, and fuel cell technology. Fuel cells function as electrochemical engines that convert the chemical energy released into the reaction of H<sub>2</sub> and O<sub>2</sub> and then into electrical energy. Polymer electrolyte fuel cells (PEFCs) have applications in a variety of areas such as electric vehicles and mobile devices because of their high electrical power densities and low working temperatures. However, several problems need to be solved before commercializing PEFCs. One of the most challenging tasks is related to electrodes. Pt is used for both the anode and cathode sides of PEFCs. At the anode side, H<sub>2</sub> gas is adsorbed on the surface of the Pt electrode and is transformed into protons and electrons catalyzed by Pt. One problem is caused by CO impurities contained in the fuel gas. Even if contamination is of the order of parts per million, CO molecules almost fully cover the surface of the Pt electrode and prevent H<sub>2</sub> fuel gas from reacting on the Pt surface.<sup>1</sup> This loss of catalytic function caused by CO gas is known as CO poisoning.

Bimetallic catalysts are useful due to their versatility; their catalytic activities and selectivity's can be tuned by varying properties such as composition, particle size, and support. CO oxidation on transition metal and oxide catalysts has attracted much interest in recent years. Tremendous efforts have been devoted to the removal

of CO contamination from H<sub>2</sub> fuel. Attempts to increase activity by alloying Pt with a second metal have also been reported recently. The presence of a second metal such as Ru, Sn, or Mo in the anode catalyst, either alloyed or co-deposited with Pt, has provided remarkable improvements in CO tolerance.<sup>2–7</sup> Among the many reports, Pt–Ru alloys have been studied most intensively because they are known to be the most promising electrodes for overcoming the CO poisoning problem.<sup>8–10</sup> Thus far, the alloying effects have been interpreted in terms of ligand and bifunctional effects.<sup>8,11</sup> In these mechanisms, the Ru sites act as adsorption centers for the O-containing surfaces species reacting with the CO to produce CO<sub>2</sub>. However, several authors have suggested the weakening of the CO chemisorption bonds to Pt–Ru with respect to pure Pt, which was confirmed by the recent ultrahigh vacuum (UHV) studies of Pt-modified Ru(0001) surfaces by Behm et al.<sup>12</sup> Watanabe et al. reported that, for the methanol decomposition reaction, dehydrogenation occurs at Pt sites, and the oxidation of CO proceeds at Ru sites with easily formed OH species.

Ge et al. investigated CO adsorption on Pt–Ru bulk and surface alloys. They noted that CO adsorption resulted in increased Ru–CO bond strength, whereas the Pt–CO bonds were weakened in the bulk alloy. On the other hand, both the Ru–CO and Pt–CO bonds were strengthened in the surface alloys.<sup>13</sup> Based on their comparative analysis of H adsorption on Pt(111) and Pt–Ru(111) surfaces, Pistonesi et al. showed that Ru atoms induce changes in the electronic structure of Pt, and the adsorption energy of H on the Pt–Ru alloy was significantly reduced compared to that on the Pt(111) surface.<sup>14</sup>

Contributing Editor: Susan B. Sinnott

<sup>a)</sup>Address all correspondence to this author.

e-mail: takaba@cc.kogakuin.ac.jp

DOI: 10.1557/jmr.2016.286

Orita et al. studied the adsorption characteristics of CO on Pt(111) for different calculation parameters and confirmed atop as the most preferred site.<sup>15</sup>

Koper et al. theoretically examined CO and OH adsorption on Pt–Ru alloys and reported that OH preferentially adsorbed at the Ru sites, whereas CO preferentially adsorbed at the Pt sites; they also predicted that the surface of a good catalyst must have a well-mixed distribution of Pt and Ru.<sup>16</sup> In a density functional theory (DFT) study of the adsorption phenomena of CO and H<sub>2</sub> on different Pt-based binary alloys, Shimodaira et al. reported that Pt atoms were enriched in the surface layer of Pt–Ru alloy, which was suggested by experimental work.<sup>17</sup> In the CO electro-oxidation process, alloying Pt with Ru or Sn provides new surface sites that are better than the Pt sites at dissociation.<sup>18</sup> In a theoretical study of CO oxidation on Pt and PtMo, Ji et al. reported that the barrier to CO oxidation on PtMo surfaces is lower than that on pure Pt.<sup>19</sup> This same group also reported that OH is much more localized on PtMo than on pure Pt, increasing the probability of OH reacting with CO.<sup>20</sup>

Koper et al. investigated the bonding mechanisms of water dissociation products (i.e., H, O, and OH) on various metal surfaces and observed that when an electric field was applied, O and OH adsorbates donated some electric charge to the surface; however, the effect of an applied electric field on H adsorption was negligible.<sup>21</sup> Han et al. investigated the coadsorption of CO with O or OH on Pt and Pt–Ru alloys and noted that when Ru was oxidized by O or OH, the Pt–CO bond strength changed dramatically.<sup>22</sup> Some experimental studies have reported that the ratio of Pt to Ru is important in the design of efficient anode catalysts; these studies suggested that Pt:Ru = 2:3 is a good composition for CO-tolerant anode catalysts.<sup>23–25</sup> They reported on particle size and composition on CO tolerance at Pt<sub>2</sub>Ru<sub>3</sub>/C investigated by in situ attenuated total reflection Fourier-transform infrared<sup>24</sup> and structures of anode catalysts were analyzed by extended x-ray absorption fine structure spectroscopy.<sup>25</sup> The mechanisms of CO tolerance are thought to involve the adsorption of O-containing species (OH) at Ru sites so that CO adsorbed at Pt sites can participate in the bimolecular reaction with activated O species. Ishikawa et al. reported from their theoretical study that a secondary metal (M) is necessary for activating H<sub>2</sub>O which produce OH and from the CO<sub>ads(Pt)</sub> + OH<sub>ads(M)</sub> combination reactions and predicted the best alloying metal with Pt for CO oxidation.<sup>26</sup> The adsorption of CO and OH on Pt–Ru alloys with different Pt-to-Ru mixing ratios has been theoretically studied<sup>16,27</sup>; however, those theoretical studies did not consider the mixing ratio of Pt:Ru = 2:3 and also still not clear the atomic conformation (Pt–Pt, Ru–Ru, Pt–Ru) in the active sites on metal surface which can accelerate CO oxidation.

In this paper, we report the results of DFT calculations on the interactions of H, CO, and OH with the Pt<sub>2</sub>Ru<sub>3</sub> alloy surface. Since the stoichiometry of Pt<sub>2</sub>Ru<sub>3</sub> alloy has not been studied theoretically, different active pair sites (Pt–Pt, Pt–Ru, and Ru–Ru) that may affect the adsorption properties of adsorbates on the surface and subsurface were investigated in this study. The results of the quantum chemical calculations provide information that will be valuable in correctly interpreting experimental results as well as a direction for modeling large-scale molecular systems, which can help to predict realistic phenomena quantitatively.

## II. METHODS

DFT calculations were performed with program package DMol<sup>3</sup> in Materials Studio supplied by BIOVIA, Inc.<sup>28–30</sup> The physical wave functions were expanded in terms of accurate numerical basis sets. The effective core potential and double numerical basis with polarization functions basis set were chosen for all calculations. The generalized gradient approximation functional developed by Perdew–Burke–Ernzerhof<sup>31</sup> was used. The convergence tolerances for energy, maximum force, and maximum displacement were less than 1.0 × 10<sup>-5</sup> Ha, 0.002 Ha/Å, and 0.005 Ha/Å, respectively. The K-point mesh was set to 2 × 2 × 1. The adsorption energies of the adsorbates were computed by subtracting the energies of the gas phase (H, CO, and OH) and surface from the energy of the adsorption system:

$$E_{ad} = E(\text{gas}/\text{surface}) - E(\text{gas}) - E(\text{surface}) \quad ,$$

where gas = H, CO, and OH. With this definition, a negative  $E_{ad}$  corresponds to stable adsorption on the surface. All of the calculations were carried out in the spin-unrestricted mode.

We performed the periodic slab calculations considering Pt<sub>2</sub>Ru<sub>3</sub>(111) alloys as having ordered face-centered cubic (fcc) structures. The metal alloy Pt<sub>2</sub>Ru<sub>3</sub>(111) slab consisted of five layers. We prepared various models with different conformations of Pt and Ru atoms while keeping Pt:Ru = 2:3. A periodic five-layer slab with four atoms per layer was modeled to represent a 2 × 2 unit cell, and it was expanded to create a vacuum phase with a thickness of about 10 Å above the (111) surface. The metal atoms in the bottom three layers of the slab were fixed at their positions, while the metal atoms in the top two layers and the adsorbate (CO, H, OH) atoms were allowed to relax in the subsequent geometry optimization and energy calculations. The cell parameters for all models were  $a = b = 5.5492$  Å,  $c = 19.05$  Å,  $\alpha = \beta = 90^\circ$ , and  $\gamma = 120^\circ$ . The calculated nearest-neighbor Pt–Ru bond distance in our Pt<sub>2</sub>Ru<sub>3</sub>(111) alloy surface was 2.759 Å, which is in good agreement with previously reported

theoretical values<sup>16,27</sup>; the previously reported bulk lattice constants were 2.756 Å for PtRu<sub>2</sub> and 2.78 Å for Pt<sub>2</sub>Ru,<sup>16,27</sup> although the mixing Pt:Ru mixing ratio in our system was slightly different.

### III. RESULTS AND DISCUSSION

#### A. Adsorption of H

Table I lists the binding energies and equilibrium distances for H adsorption at the atop, bridge, and hollow sites on the Pt<sub>2</sub>Ru<sub>3</sub> surface for different conformations of Pt and Ru atoms. In the five-layer Pt<sub>2</sub>Ru<sub>3</sub> surface, the top two layers are composed of Pt and Ru atoms with the same ratio but different conformations of Pt and Ru atoms (Fig. 1). In the metal alloy, atomic conformations of the top two layers in Fig. 1 are [a(i–iv)] Pt<sub>4</sub>/Ru<sub>4</sub>, Ru<sub>4</sub>/Pt<sub>4</sub>, [b(i–iv)] Pt<sub>2</sub>Ru<sub>2</sub>/Pt<sub>2</sub>Ru<sub>2</sub>, [c(i–iv)] Pt<sub>3</sub>Ru<sub>1</sub>/Pt<sub>1</sub>Ru<sub>3</sub>, and [d(i–iv)] Ru<sub>3</sub>Pt<sub>1</sub>/Pt<sub>3</sub>Ru<sub>1</sub>. Top view of the top two layers shown in [Figs. 1(a–i<sup>–</sup>)], 1(a–i<sup>–</sup>), 1(b–i<sup>–</sup>), 1(c–i<sup>–</sup>), and 1(d–i<sup>–</sup>)] to visualize adsorption sites clearly. In Figs. 1(a–i<sup>–</sup>) and 1(a–i<sup>–</sup>), top surface is covered with homogenous Pt and Ru atom, respectively. On the other hand, in Figs. 1(b–i<sup>–</sup>), 1(c–i<sup>–</sup>), and 1(d–i<sup>–</sup>), Pt/Ru atom ratio of the top surfaces are 2:2, 3:1, and 1:3, respectively. Of course there are number of combinations possible but in this study for H adsorption, we considered the adsorption sites for only the above-mentioned mixing combinations. Based on the adsorption energies of H on the Pt<sub>2</sub>Ru<sub>3</sub> surfaces, for most surface compositions, H preferably adsorbed on the hollow sites compared to the atop and bridge sites which follow previous report by Ishikawa et al. about adsorption phenomena of hydrogen at the Pt(111)/water surface.<sup>32</sup> The calculated adsorption energies of H on the Pt<sub>4</sub>/Ru<sub>4</sub> surface are –2.580, –2.422, and –2.612 eV for atop (Pt site), bridge site, and hollow site, respectively [Figs. 1(a–i) and 1(a–ii)], and hollow site is not shown here. The adsorption energies of H on the Ru<sub>4</sub>/Pt<sub>4</sub> are –2.778, –3.156, and –3.159 eV for the atop (Ru), bridge (Ru–Ru), and hollow sites (not shown in figure), which are summarized in Table I. The calculated

adsorption energies of H on the Pt site of the Pt<sub>4</sub>/Ru<sub>4</sub> surface are in excellent agreement with experimental value of –2.64 eV and with previously reported theoretical values.<sup>21,33</sup> The adsorption energies of H on the Pt<sub>2</sub>Ru<sub>2</sub>/Pt<sub>2</sub>Ru<sub>2</sub> surface for the atop (Pt), atop (Ru), bridge (Pt–Ru), and hollow sites, respectively, are shown in Figs. 1[b(i)–b(iv)] and Table I. We also

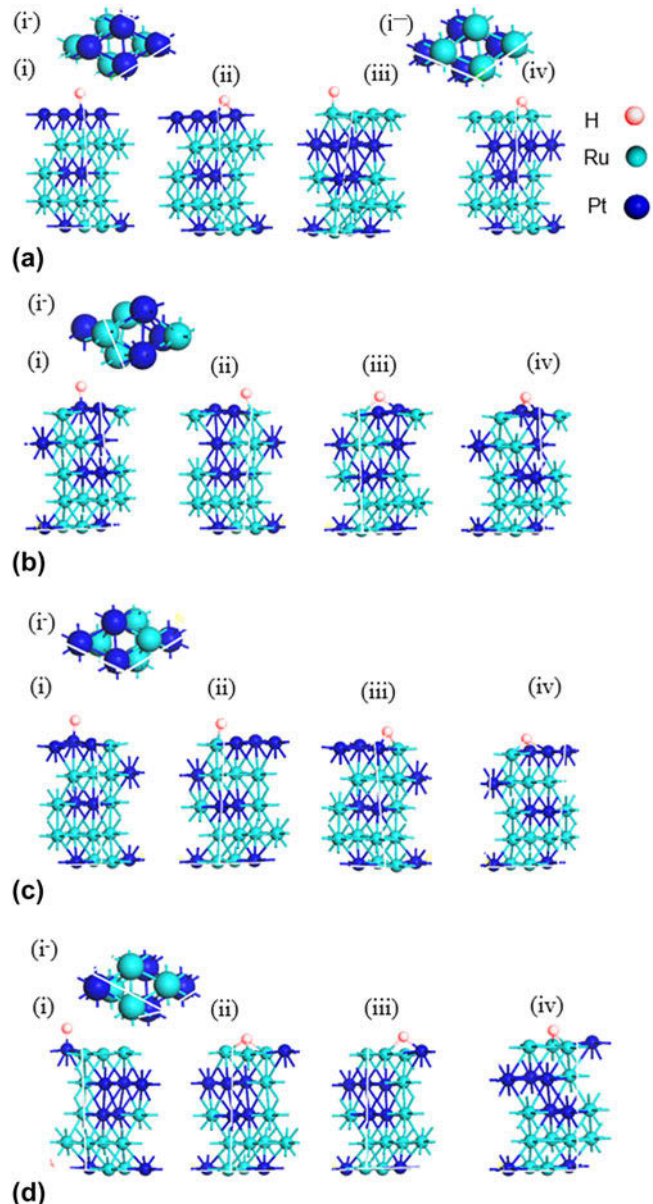


TABLE I. Calculated adsorption energies  $E_{\text{ads}}$  (in eV) for H adsorbed on atop, bridge, and hollow sites on Pt<sub>2</sub>Ru<sub>3</sub>.

Metal surface (atomic conformations of the top two layers)	$E_{\text{ads}}$ (eV) and bond distance (Å)					
	Atop site					
	Site (Pt)	Pt–H (Å)	Site (Ru)	Ru–H (Å)	Bridge site	Hollow site
(Pt <sub>4</sub> /Ru <sub>4</sub> )	–2.580	1.591	...	...	–2.422	–2.612
(Ru <sub>4</sub> /Pt <sub>4</sub> )	...	...	–2.778	1.612	–3.156	–3.159
(Pt <sub>2</sub> Ru <sub>2</sub> /Pt <sub>2</sub> Ru <sub>2</sub> )	–2.755	1.571	–2.519	1.622	–2.775	–2.669
(Pt <sub>3</sub> Ru <sub>1</sub> /Pt <sub>1</sub> Ru <sub>3</sub> )	–2.664	1.580	–2.658	1.624	–2.653	–2.689
(Pt <sub>1</sub> Ru <sub>3</sub> /Pt <sub>3</sub> Ru <sub>1</sub> )	–2.831	1.573	–2.735	1.610	–2.897	–2.386

FIG. 1. Adsorption models of H on Pt<sub>2</sub>Ru<sub>3</sub>: (a) (i<sup>–</sup>) top view for Pt<sub>4</sub>/Ru<sub>4</sub>, (i<sup>–</sup>) top view for Ru<sub>4</sub>/Pt<sub>4</sub>, H adsorption on Pt<sub>4</sub>/Ru<sub>4</sub> and Ru<sub>4</sub>/Pt<sub>4</sub> at, (i) Pt atop, (ii) bridge, (iii) Ru atop, and (iv) bridge sites; (b) (i<sup>–</sup>) top view for Pt<sub>2</sub>Ru<sub>2</sub>/Pt<sub>2</sub>Ru<sub>2</sub>, H adsorption on Pt<sub>2</sub>Ru<sub>2</sub>/Pt<sub>2</sub>Ru<sub>2</sub> at (i) Pt atop, (ii) Ru atop, (iii) bridge, and (iv) hollow sites; (c) (i<sup>–</sup>) top view for Pt<sub>3</sub>Ru<sub>1</sub>/Pt<sub>1</sub>Ru<sub>3</sub>, H adsorption on Pt<sub>3</sub>Ru<sub>1</sub>/Pt<sub>1</sub>Ru<sub>3</sub> at (i) Pt atop, (ii) Ru atop, (iii) bridge, and (iv) hollow sites; and (d) (i<sup>–</sup>) top view for Pt<sub>1</sub>Ru<sub>3</sub>/Pt<sub>3</sub>Ru<sub>1</sub>, H adsorption on Pt<sub>1</sub>Ru<sub>3</sub>/Pt<sub>3</sub>Ru<sub>1</sub> at (i) Pt atop, (ii) Ru atop, (iii) bridge, and (iv) hollow sites.

calculated the adsorption energies of H on the  $\text{Pt}_3\text{Ru}_1/\text{Pt}_1\text{Ru}_3$  and  $\text{Pt}_1\text{Ru}_3/\text{Pt}_2\text{Ru}_1$  surfaces at the atop (Pt), atop (Ru), bridge (Pt–Ru), and hollow sites (Table I). From the adsorption energies of H on the  $\text{Pt}_2\text{Ru}_3$  surfaces with different conformations of Pt and Ru atoms, we note an energetically stable H– $\text{Pt}_2\text{Ru}_3$  complex for adsorption at the hollow site.

The optimized structures are confirmed from the calculated Pt–H and Ru–H bond distances in the H– $\text{Pt}_2\text{Ru}_3$  complex and also from the adsorption strength of H at the Pt or Ru site. For adsorption at the atop site, H preferentially adsorbed at the Pt site rather than at the Ru site. The calculated Pt–H bond distances on the  $\text{Pt}_2\text{Ru}_3$  surface are listed in Table I which obtained from the optimized structure in Figs. 1(a-i), 1(b-i), 1(c-i), and 1(d-i), respectively. On the other hand, the calculated Ru–H bond distances on the  $\text{Pt}_2\text{Ru}_3$  complex are shown Table I which obtained from the optimized structures in Figs. 1(a-iii), 1(b-ii), 1(c-ii), and 1(d-ii), respectively. If H was located on the bridge site (Pt–Ru) in the initial structure, H bent slightly toward the Pt sites in the optimized structure, as shown Figs. 1(b-iii), 1(c-iii), and 1(d-iii). For Fig. 1(c-iii) model, the measured bond distances are 1.759 Å for Pt–H and 1.889 Å for Ru–H, clearly indicating that H preferentially adsorbed at the Pt sites on the surface. From the adsorption energies and bond distances of Pt–H and Ru–H, we confirmed that H adsorbed preferentially at the Pt sites compared to the Ru sites. The DFT results also confirmed that the stable site for H adsorption depends not only on the adsorption site, but also on the atoms neighboring of the adsorption site and the subsurface. A conformation with a top surface containing both Pt and Ru atoms but with more Pt and a second layer rich in Ru is most stable conformation for H adsorption among the investigated H– $\text{Pt}_2\text{Ru}_3$  systems shown in Table I.

## B. Adsorption of CO

Five types of  $\text{Pt}_2\text{Ru}_3$  alloys with different conformations of Pt and Ru atoms are depicted in Fig. 2. Table II shows the calculated adsorption energies of CO on the  $\text{Pt}_2\text{Ru}_3$  alloy surfaces with different conformations of Pt and Ru atoms. Using DFT, we simulated the CO adsorption phenomena on all five of the surfaces. On the  $\text{Pt}_2\text{Ru}_3$  alloy surface, we considered different adsorption sites, as shown in Figs. 2(a)–2(d). From the results summarized in Table II, the calculated adsorption energies of CO at the Pt sites of the  $\text{Pt}_4/\text{Ru}_4$ ,  $\text{Pt}_2\text{Ru}_2/\text{Pt}_2\text{Ru}_2$ ,  $\text{Pt}_3\text{Ru}_1/\text{Pt}_1\text{Ru}_3$ , and  $\text{Ru}_3\text{Pt}_1/\text{Pt}_3\text{Ru}_1$  surfaces of the  $\text{Pt}_2\text{Ru}_3$  alloy are –1.380, –1.473, –1.407, and –1.617 eV, respectively.

The adsorption energies at the atop (Ru site) are –2.569, –2.163, –2.138, and –2.522 eV, on the  $\text{Ru}_4/\text{Pt}_4$ ,  $\text{Pt}_2\text{Ru}_2/\text{Pt}_2\text{Ru}_2$ ,  $\text{Pt}_3\text{Ru}_1/\text{Pt}_1\text{Ru}_3$ , and  $\text{Ru}_3\text{Pt}_1/\text{Pt}_3\text{Ru}_1$

surfaces, respectively. The calculated adsorption energies of CO on the bridge sites are –1.093 eV (Pt–Pt), –2.397 eV (Ru–Ru), –2.163 eV (Pt–Ru), –2.126 eV (Pt–Ru), and –2.035 eV (Pt–Ru) for the  $\text{Pt}_4/\text{Ru}_4$ ,  $\text{Ru}_4/\text{Pt}_4$ ,  $\text{Pt}_2\text{Ru}_2/\text{Pt}_2\text{Ru}_2$ ,  $\text{Pt}_3\text{Ru}_1/\text{Pt}_1\text{Ru}_3$ , and  $\text{Ru}_3\text{Pt}_1/\text{Pt}_3\text{Ru}_1$  surfaces, respectively, as shown in Figs. 2(a-ii), 2(a-iv), 2(b-iii), 2(c-iii), and 2(d-iii), respectively. The corresponding adsorption energies at the hollow sites are summarized in Table II. These calculated adsorption energies indicate that the atop site (CO–Ru) is the most stable.

The CO adsorption on the bridge site for all combinations in which the surface was covered by Pt and Ru can be explained by the fact that in the optimized structure, CO moves to the Ru site from the initial Pt site, which indicates higher affinity of CO to the Ru site than to the Pt site as shown in Figs. 2(b-iii), 2(c-iii), and 2(d-iii). The CO adsorption strength at the atop sites (Ru) of the  $\text{Ru}_4/\text{Pt}_4$  and  $\text{Ru}_3\text{Pt}_1/\text{Pt}_3\text{Ru}_1$  conformation of top two layers were higher than those at the same adsorption sites of other surface conformation (Table II) because both  $\text{Ru}_4/\text{Pt}_4$  and  $\text{Ru}_3\text{Pt}_1/\text{Pt}_3\text{Ru}_1$  conformations, top surfaces were fully covered with Ru or with Ru rich as shown in Figs. 2(a-iii) and 2(d-iii). There were noticeable changes in the internal bond length of chemisorbed CO on the  $\text{Pt}_2\text{Ru}_3$  alloy. The calculated equilibrium bond distances of C–O when adsorbed at the Pt sites on  $\text{Pt}_2\text{Ru}_3$  for different combinations of Pt and Ru in the top two layers are listed in Table II that were obtained from the optimized CO– $\text{Pt}_2\text{Ru}_3$  complex are shown in Figs. 2(a-i), 2(b-i), 2(c-i), and 2(d-i), respectively. On the other hand, the calculated equilibrium bond distances of C–O at the Ru sites are summarized in Table II, on the same surfaces, from the optimized structure shown in Figs. 2(a-iii), 2(b-ii), 2(c-ii), and 2(d-ii), respectively. The measured bond distances of CO indicate that CO preferentially adsorbed at the Ru sites. In addition, CO adsorption on the  $\text{Pt}_2\text{Ru}_3$  alloy not only depended on the adsorption site, but also on the natures of the neighboring atoms and the subsurface atomic combination. The calculated adsorption strength of CO on the  $\text{Pt}_2\text{Ru}_3$  alloy and the change in the internal bond distance of adsorbed CO indicated that the Ru-rich top surface is the most stable conformation of the CO– $\text{Pt}_2\text{Ru}_3$  complex.

## C. Adsorption of OH

As mentioned in the introduction, the mechanisms of CO tolerance are believed to involve the adsorption of O-containing species (OH) at Ru sites. The DFT-computed adsorption energies and equilibrium bond distances of OH with  $\text{Pt}_2\text{Ru}_3$  alloy surfaces for different combinations of Pt and Ru atoms are listed in Table III. In our calculations, we considered the atop, bridge, and hollow sites for OH adsorption on alloy surfaces with different

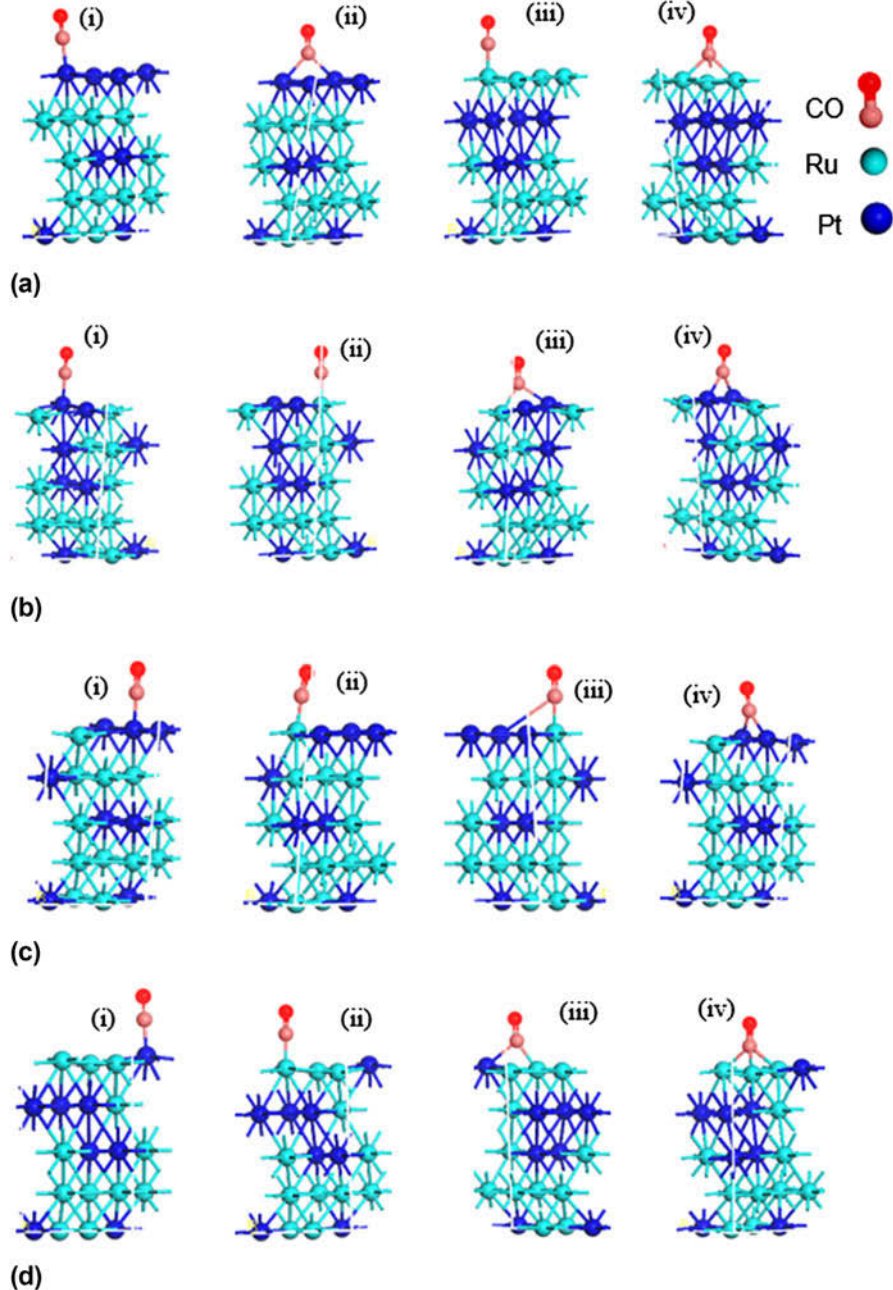


FIG. 2. Adsorption models of CO on  $\text{Pt}_2\text{Ru}_3$ : (a) CO adsorption on  $\text{Pt}_4/\text{Ru}_4$ ,  $\text{Ru}_4/\text{Pt}_4$  at (i) Pt atop, (ii)  $\text{Pt}_4/\text{Ru}_4$  bridge, (iii) Ru atop, and (iv)  $\text{Ru}_4/\text{Pt}_4$  bridge sites; (b) CO adsorption on  $\text{Pt}_2\text{Ru}_2/\text{Pt}_2\text{Ru}_2$  at (i) Pt atop, (ii) Ru atop, (iii) bridge, and (iv) hollow sites; (c) CO adsorption on  $\text{Pt}_3\text{Ru}_1/\text{Pt}_1\text{Ru}_3$  at (i) Pt atop, (ii) Ru atop, (iii) bridge, and (iv) hollow sites; and (d) CO adsorption on  $\text{Pt}_1\text{Ru}_3/\text{Pt}_3\text{Ru}_1$  at (i) Pt atop, (ii) Ru atop, (iii) bridge, and (iv) hollow sites.

combinations of Pt and Ru [Figs. 3(a)–3(d)]. In the  $\text{Pt}_2\text{Ru}_3$  alloy, there are five possible conformations of Pt and Ru atoms. We considered OH adsorption at the Pt, Ru, bridge, and hollow sites of the  $\text{Pt}_2\text{Ru}_3$  alloy. The calculated adsorption energies of OH on the Pt atop sites on the  $\text{Pt}_4/\text{Ru}_4$ ,  $\text{Pt}_2\text{Ru}_2/\text{Pt}_2\text{Ru}_2$ ,  $\text{Pt}_3\text{Ru}_1/\text{Pt}_1\text{Ru}_3$ , and  $\text{Ru}_3\text{Pt}_1/\text{Pt}_3\text{Ru}_1$  surfaces of the  $\text{Pt}_2\text{Ru}_3$  alloy are shown in Table III. On the other hand, the adsorption energies at the Ru atop sites are summarized (Table III), on the

$\text{Ru}_4/\text{Pt}_4$ ,  $\text{Pt}_2\text{Ru}_2/\text{Pt}_2\text{Ru}_2$ ,  $\text{Pt}_3\text{Ru}_1/\text{Pt}_1\text{Ru}_3$ , and  $\text{Ru}_3\text{Pt}_1/\text{Pt}_3\text{Ru}_1$  surfaces, respectively. In the OH adsorption at the bridge site (Pt–Ru) of the optimized structure, OH moves to the Ru site from the Pt site, as noted in Figs. 3(b-iii), 3(c-iii), and 3(d-iii). The calculated adsorption energies of OH on the  $\text{Pt}_4/\text{Ru}_4$ ,  $\text{Ru}_4/\text{Pt}_4$ ,  $\text{Pt}_2\text{Ru}_2/\text{Pt}_2\text{Ru}_2$ ,  $\text{Pt}_3\text{Ru}_1/\text{Pt}_1\text{Ru}_3$ , and  $\text{Ru}_3\text{Pt}_1/\text{Pt}_3\text{Ru}_1$  surfaces at the bridge sites and at the hollow sites are summarized in Table III. The calculated adsorption energies indicate that OH is preferentially

TABLE II. Calculated adsorption energies  $E_{\text{ads}}$  (in eV) for CO adsorbed on atop, bridge, and hollow sites on  $\text{Pt}_2\text{Ru}_3$ .

Metal surface (atomic conformations of the top two layers)	$E_{\text{ads}}$ (eV) and bond distance (Å)					
	Atop site					
	Site (Pt)	C–O (Å)	Site (Ru)	C–O (Å)	Bridge site	Hollow site
( $\text{Pt}_4/\text{Ru}_4$ )	−1.380	1.160	...	...	−1.093	−1.204
( $\text{Ru}_4/\text{Pt}_4$ )	...	...	−2.569	1.175	−2.397	−2.466
( $\text{Pt}_2\text{Ru}_2/\text{Pt}_2\text{Ru}_2$ )	−1.473	1.163	−2.163	1.170	−2.163	−1.626
( $\text{Pt}_3\text{Ru}_1/\text{Pt}_1\text{Ru}_3$ )	−1.407	1.162	−2.138	1.170	−2.126	−1.502
( $\text{Pt}_1\text{Ru}_3/\text{Pt}_3\text{Ru}_1$ )	−1.617	1.164	−2.522	1.176	−2.035	−2.247

TABLE III. Calculated adsorption energies  $E_{\text{ads}}$  (in eV) for OH adsorbed on atop, bridge, and hollow sites on metal  $\text{Pt}_2\text{Ru}_3$ .

Metal surface (atomic conformations of the top two layers)	$E_{\text{ads}}$ (eV) and bond distance (Å)					
	Atop site					
	Site (Pt)	O–H (Å)	Site (Ru)	O–H (Å)	Bridge site	Hollow site
( $\text{Pt}_4/\text{Ru}_4$ )	−2.113	0.979	...	...	−1.976	−2.035
( $\text{Ru}_4/\text{Pt}_4$ )	...	...	−2.993	0.982	−3.295	−3.400
( $\text{Pt}_2\text{Ru}_2/\text{Pt}_2\text{Ru}_2$ )	−2.146	0.980	−2.702	0.981	−2.975	−2.765
( $\text{Pt}_3\text{Ru}_1/\text{Pt}_1\text{Ru}_3$ )	−2.104	0.979	−2.752	0.992	−2.750	−2.745
( $\text{Pt}_1\text{Ru}_3/\text{Pt}_3\text{Ru}_1$ )	−2.750	0.981	−2.978	0.989	−3.158	−3.482

absorbed at the hollow sites. For the model shown in Fig. 3(a–iv), in which the top surface was fully covered with Ru atoms, the calculated adsorption energy was −3.400 eV. In another system in which the first two layers were  $\text{Ru}_3\text{Pt}_1/\text{Pt}_3\text{Ru}_1$ , the calculated energy is −3.482 eV, indicating that the Ru-rich top surface was preferable for OH adsorption. In our previous study, for pure Pt and pure Ru, OH binding to Ru sites was almost 1.5 times stronger than the binding to Ru sites.<sup>34</sup> The adsorption energy of OH depends not only on the adsorption site, but also on the subsurface. These adsorption characteristics of OH on  $\text{Pt}_2\text{Ru}_3$  agree with the theoretical observations of OH adsorption on Pt–Ru.<sup>16</sup>

The geometric change of absorbed OH reveals a general correlation between O–H distance and calculated adsorption energy, although there are some deviations in this trend due to the size limitations of the system. The equilibrium bond distances of O–H at the Pt site are 0.979 Å, 0.980 Å, 0.979 Å, and 0.981 Å when the first two layers in the  $\text{Pt}_2\text{Ru}_3$  surface are  $\text{Pt}_4/\text{Ru}_4$ ,  $\text{Pt}_2\text{Ru}_2/\text{Pt}_2\text{Ru}_2$ ,  $\text{Pt}_3\text{Ru}_1/\text{Pt}_1\text{Ru}_3$ , and  $\text{Ru}_3\text{Pt}_1/\text{Pt}_3\text{Ru}_1$ , respectively; on the other hand, the corresponding O–H bond distances for adsorption at the Ru site are 0.982, 0.981, 0.992, and 0.989 Å, respectively. Tables II and III indicate nearly the same trends for both OH and CO adsorption on the  $\text{Pt}_2\text{Ru}_3$  alloy surfaces. Our analysis indicates that the adsorption properties of OH depend on the adsorption site,

the natures of the atoms neighboring the adsorption site, and the subsurface atomic arrangement.

#### D. CO coadsorption with OH and H

OH is another important chemical species in the oxidation of CO; it is observed experimentally as an intermediate of water dissociation on a Pt electrode. In the bifunctional mechanism, OH plays an important role as an adsorbate that facilitates CO oxidation by providing a source of O on the surface.<sup>35,36</sup> In Sec. III. A, III. B, and III. C, we discussed the separate adsorption phenomena of H, CO, and OH, respectively, on different surfaces. To study the coadsorption of CO and OH, we considered two types of  $\text{Pt}_2\text{Ru}_3$  alloy surfaces (Fig. 4). Both adsorbates were placed at the atop sites, as shown in Figs. 4(a)–4(e). The calculated adsorption energies are listed in Table IV and compared to the CO and OH coadsorption energies. The calculated adsorption energies of CO in the presence of coadsorbate OH are summarized (Table IV), when the first two layers of the  $\text{Pt}_2\text{Ru}_3$  surface were  $\text{Pt}_4/\text{Ru}_4$ ,  $\text{Pt}_3\text{Ru}_1/\text{Pt}_1\text{Ru}_3$ ,  $\text{Pt}_2\text{Ru}_2/\text{Pt}_2\text{Ru}_2$ ,  $\text{Ru}_3\text{Pt}_1/\text{Pt}_3\text{Ru}_1$ , and  $\text{Ru}_4/\text{Pt}_4$ , respectively [Figs. 4(a)–4(e)]. Table IV indicates that the adsorption energies of CO were decreased for coadsorption with OH compared to CO-only adsorption at the same adsorption sites.

We also considered the adsorption energies of OH on different surfaces in the presence of CO and found that the adsorption energies of both Pt–OH and Pt–CO decreased. The calculated adsorption energies of OH in the presence of CO on  $\text{Pt}_4/\text{Ru}_4$ ,  $\text{Pt}_3\text{Ru}_1/\text{Pt}_1\text{Ru}_3$ ,  $\text{Pt}_2\text{Ru}_2/\text{Pt}_2\text{Ru}_2$ ,  $\text{Ru}_3\text{Pt}_1/\text{Pt}_3\text{Ru}_1$ , and  $\text{Ru}_4/\text{Pt}_4$  conformations [Figs. 4(a)–4(e)], and in most cases, the adsorption strength of OH on  $\text{Pt}_2\text{Ru}_3$  decreased in the presence of CO (Table IV). The coadsorption energies of OH at the Ru sites (−2.653, −2.317, and −2.827 eV) and Pt sites (−1.985 and −1.908 eV) indicate that OH preferentially adsorbed at the Ru site compared to at the Pt site. The results suggest that if only a single species (CO or OH) adsorbed on the  $\text{Pt}_2\text{Ru}_3$  surface, it would preferentially be adsorbed at the Ru sites. In contrast, for the coadsorption of CO and OH, OH preferentially bound to the Ru-rich sites [Figs. 4(d) and 4(e)]. For coadsorption on the  $\text{Pt}_4/\text{Ru}_4$  surface, the Pt–CO bond strength was −1.254 eV, while the Pt–CO strength was −1.424 eV for the  $\text{Pt}_2\text{Ru}_2/\text{Pt}_2\text{Ru}_2$  surface.

To study the coadsorption of CO with atomic hydrogen, we calculated the adsorption energies for models in which H and OH were placed at the Pt or Ru sites [Figs. 5(a)–5(e)]. The calculated coadsorption energies of CO with H are shown in Table V for the  $\text{Pt}_4/\text{Ru}_4$ ,  $\text{Pt}_3\text{Ru}_1/\text{Pt}_1\text{Ru}_3$ ,  $\text{Pt}_2\text{Ru}_2/\text{Pt}_2\text{Ru}_2$ ,  $\text{Ru}_3\text{Pt}_1/\text{Pt}_3\text{Ru}_1$ ,  $\text{Ru}_4/\text{Pt}_4$  surface conformations of  $\text{Pt}_2\text{Ru}_3$ . These results indicate that the adsorption energy of CO on  $\text{Pt}_2\text{Ru}_3$  decreased in the presence of H for all surface conformations. We also

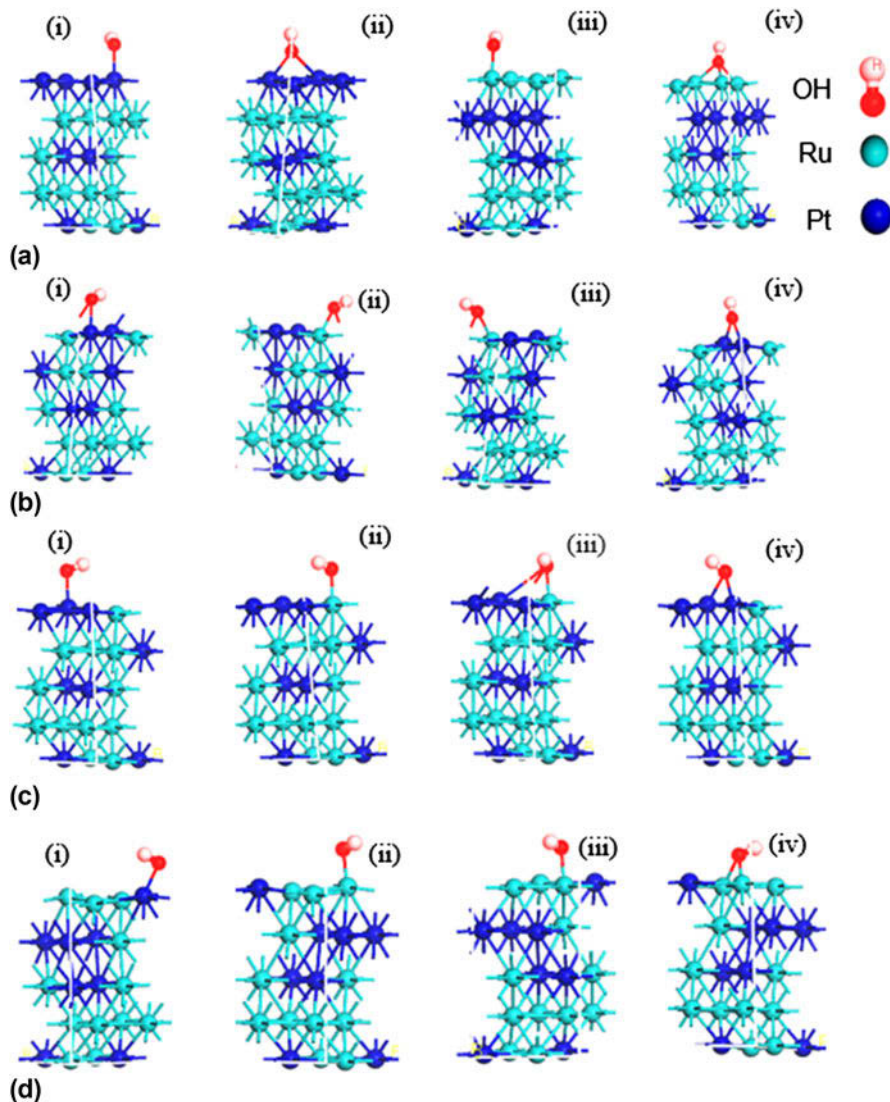


FIG. 3. Adsorption models of OH on  $\text{Pt}_2\text{Ru}_3$ : (a) OH adsorption on  $\text{Pt}_4/\text{Ru}_4$ ,  $\text{Ru}_4/\text{Pt}_4$  at (i) Pt atop, (ii) Pt bridge, (iii) Ru atop, and (iv) bridge sites; (b) OH adsorption on  $\text{Pt}_2\text{Ru}_2/\text{Pt}_2\text{Ru}_2$  at (i) Pt atop, (ii) Ru atop, (iii) bridge, and (iv) hollow sites; (c) OH adsorption on  $\text{Pt}_3\text{Ru}_1/\text{Pt}_1\text{Ru}_3$  at (i) Pt atop, (ii) Ru atop, (iii) bridge, and (iv) hollow sites; and (d) OH adsorption  $\text{Pt}_1\text{Ru}_3/\text{Pt}_3\text{Ru}_1$  at (i) Pt atop, (ii) Ru atop, (iii) bridge, and (iv) hollow sites.

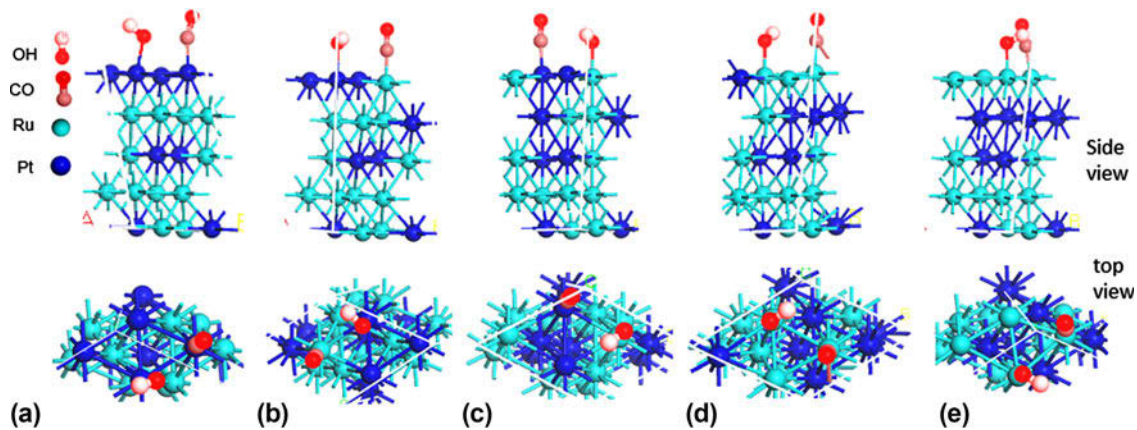


FIG. 4. Coadsorption models of CO with OH on  $\text{Pt}_2\text{Ru}_3$ : (a) both CO and OH coadsorb on  $\text{Pt}_4/\text{Ru}_4$  at Pt sites; (b) CO and OH coadsorb on  $\text{Pt}_3\text{Ru}_1/\text{Pt}_1\text{Ru}_3$  with OH at Pt site and CO at Ru site; (c) CO and OH coadsorb on  $\text{Pt}_2\text{Ru}_2/\text{Pt}_2\text{Ru}_2$  with OH at Ru site and CO at Pt site; (d) both CO and OH coadsorb on  $\text{Pt}_1\text{Ru}_3/\text{Pt}_3\text{Ru}_1$  at Ru site; and (e) both CO and OH coadsorb on  $\text{Ru}_4/\text{Pt}_4$  at Ru site.

calculated the adsorption energies of H in the presence of CO; the energies are summarized (Table V) for the Pt<sub>4</sub>/Ru<sub>4</sub>, Pt<sub>3</sub>Ru<sub>1</sub>/Pt<sub>1</sub>Ru<sub>3</sub>, Pt<sub>2</sub>Ru<sub>2</sub>/Pt<sub>2</sub>Ru<sub>2</sub>, Ru<sub>3</sub>Pt<sub>1</sub>/Pt<sub>3</sub>Ru<sub>1</sub>, and Ru<sub>4</sub>/Pt<sub>4</sub> conformations, respectively. These results indicate that the adsorption energy of H on Pt<sub>2</sub>Ru<sub>3</sub> decreased in the presence of CO for all surface conformations shown in Fig. 5. In addition, CO preferentially adsorbed at Ru or Ru-rich sites, while the H species preferred to be located at Pt or Pt-rich surface sites.

In general, the adsorption and coadsorption energies of H, CO, and OH on Pt<sub>2</sub>Ru<sub>3</sub> indicate that CO and OH preferentially adsorbed at Ru sites, whereas H

preferentially adsorbed at Pt sites. In our previous study,<sup>37</sup> we have investigated the stability of Pt<sub>2</sub>Ru<sub>3</sub> alloy for bare surfaces and noticed that the Pt energetically prefer to stay on the surface, while the alloying atoms Ru favor to stay on the subsurface which agrees well with the study of surface segregation energies of different metal alloys by Nørskov group using tight binding and linear muffin tin orbital method.<sup>38</sup> In this current study, we also noticed in presence of different adsorbents stability of the Pt<sub>2</sub>Ru<sub>3</sub> alloy and ratio of the alloying atoms on the surface and subsurface depends on the adsorption strength of adsorbents to the alloying atoms.

TABLE IV. Calculated coadsorption energies  $E_{\text{cads}}$  (in eV) of CO with OH on Pt<sub>2</sub>Ru<sub>3</sub>.

Metal surface (atomic conformations of the top two layers)	CO adsorption energy (eV)		OH adsorption energy (eV)	
	CO adsorption energy (Pt or Ru site)	Coadsorption of CO with OH	OH adsorption energy (Pt or Ru site)	Coadsorption of OH with CO
(Pt <sub>4</sub> /Ru <sub>4</sub> )	-1.380 (Pt)	-1.254	-2.113 (Pt)	-1.985
(Pt <sub>3</sub> Ru <sub>1</sub> /Pt <sub>1</sub> Ru <sub>3</sub> )	-2.138 (Ru)	-1.942	-2.104 (Pt)	-1.908
(Pt <sub>2</sub> Ru <sub>2</sub> /Pt <sub>2</sub> Ru <sub>2</sub> )	-1.473 (Pt)	-1.424	-2.702 (Ru)	-2.653
(Pt <sub>1</sub> Ru <sub>3</sub> /Pt <sub>3</sub> Ru <sub>1</sub> )	-2.522 (Ru)	-1.863	-2.752 (Ru)	-2.317
(Ru <sub>4</sub> /Pt <sub>4</sub> )	-2.569 (Ru)	-2.403	-2.993 (Ru)	-2.827

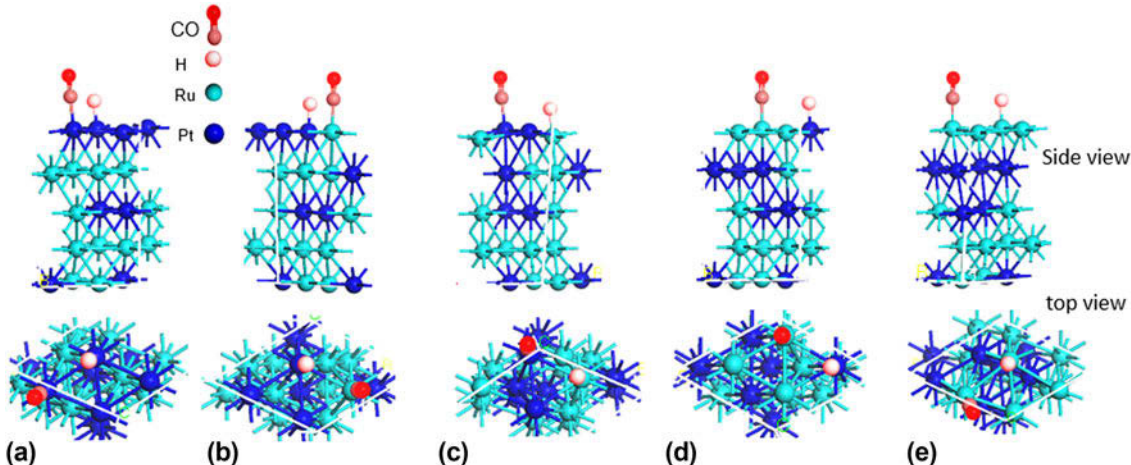


FIG. 5. Coadsorption models of CO with H on Pt<sub>2</sub>Ru<sub>3</sub>: (a) both CO and H coadsorb on Pt<sub>4</sub>/Ru<sub>4</sub> at Pt site; (b) CO and H coadsorb on Pt<sub>3</sub>Ru<sub>1</sub>/Pt<sub>1</sub>Ru<sub>3</sub> with CO at Ru site and H at Pt site; (c) CO and H coadsorb on Pt<sub>2</sub>Ru<sub>2</sub>/Pt<sub>2</sub>Ru<sub>2</sub> with CO at Pt site and H at Ru site; (d) CO and H coadsorb on Pt<sub>1</sub>Ru<sub>3</sub>/Pt<sub>3</sub>Ru<sub>1</sub> with CO at Ru site and H at Pt site; and (e) both CO and H coadsorb on Ru<sub>4</sub>/Pt<sub>4</sub> at Ru site.

TABLE V. Calculated coadsorption energies  $E_{\text{cads}}$  (in eV) of CO with H on Pt<sub>2</sub>Ru<sub>3</sub>.

Metal surface (atomic conformations of the top two layers)	CO adsorption energy (eV)		H adsorption energy (eV)	
	CO adsorption energy (Pt or Ru site)	Coadsorption of CO with H	H adsorption energy (Pt or Ru site)	Coadsorption of H with CO
(Pt <sub>4</sub> /Ru <sub>4</sub> )	-1.380 (Pt)	-1.256	-2.580 (Pt)	-2.454
(Pt <sub>3</sub> Ru <sub>1</sub> /Pt <sub>1</sub> Ru <sub>3</sub> )	-2.138 (Ru)	-2.022	-2.664 (Pt)	-2.549
(Pt <sub>2</sub> Ru <sub>2</sub> /Pt <sub>2</sub> Ru <sub>2</sub> )	-1.473 (Pt)	-1.436	-2.519 (Ru)	-2.482
(Pt <sub>1</sub> Ru <sub>3</sub> /Pt <sub>3</sub> Ru <sub>1</sub> )	-2.522 (Ru)	-1.996	-2.831 (Pt)	-2.669
(Ru <sub>4</sub> /Pt <sub>4</sub> )	-2.569 (Ru)	-2.446	-2.778 (Ru)	-2.656

Koper et al. reported that both Pt and Ru must be available on the surface of a good CO oxidation catalyst so that oxygenated species can bind to Ru sites and CO can bind to Pt sites, facilitating CO oxidation.<sup>16</sup> In our study, when the top two layers had the same mixing ratio, CO was adsorbed at the Ru sites [atop; Figs. 2(a-iii), 2(b-ii), 2(c-ii), and 2(d-ii)]. When CO coadsorbed with OH on the Pt<sub>2</sub>Ru<sub>3</sub> surface containing both Pt and Ru, OH preferentially adsorbed at the Ru sites. These observations are consistent with a previous report.<sup>16</sup> Han et al. reported that competitive adsorption at Ru and Pt sites for single Ru site with the neighboring Pt sites in that case both adsorbates (CO, OH) favor Ru site but thermodynamically favorable state has CO on the Pt site and OH on the Ru site.<sup>22</sup> Our calculation results also show a similar tendency. The calculated adsorption energies of CO in the presence OH are -1.863 and -2.403 eV on the Ru<sub>3</sub>Pt<sub>1</sub>/Pt<sub>3</sub>Ru<sub>1</sub> and Ru<sub>4</sub>/Pt<sub>4</sub> conformations, respectively, while the corresponding energies of OH in the presence of CO are -2.317 and -2.827 eV (Table IV), indicating that OH adsorption is more favorable at Ru sites compared to CO adsorption.

From the optimized structures in Fig. 2 and summarized adsorption energies of CO on the Pt<sub>2</sub>Ru<sub>3</sub> alloy, it is clearly shown that Pt–CO bond strengths decrease with increasing Pt/Ru ratio on the top surface. On the other hand, opposite behavior in case of Ru–CO adsorption strength is shown in Table II. Hence it can be concluded that well-mixed top surface with Pt rich and subsurface with Ru-rich conformation weakens adsorption strength of Pt–CO which can reduce amount of CO on the catalyst surface. These results certainly help in understanding and designing high CO-tolerance anode catalysts.

#### IV. CONCLUSION

In this paper, we presented the results of a DFT study on H, CO, and OH adsorption on Pt<sub>2</sub>Ru<sub>3</sub> (111) surfaces with a variety of Pt and Ru conformations with the goal of obtaining stable Pt<sub>2</sub>Ru<sub>3</sub> alloy for designing high CO-tolerant catalyst in PEFC. Our calculation results show that the adsorption behaviors of the investigated gases depend not only on the mixing ratio of alloying atoms, but also on the conformation of the adsorption site, the atoms neighboring the adsorption site, and the subsurface conformation. Our results indicate that the most suitable conformation for weakening the Pt–CO bond on Pt<sub>2</sub>Ru<sub>3</sub> surface covered with both Pt and Ru atoms and a second layer containing Ru. Coadsorption with either H or OH was found to decrease the CO adsorption energy for all of the investigated Pt<sub>2</sub>Ru<sub>3</sub> alloy surface conformations. For the coadsorption of CO with OH on a well-mixed Pt<sub>2</sub>Ru<sub>3</sub> surface, OH was observed to preferentially be adsorbed at Ru sites, while CO was adsorbed at Pt sites, which is important for CO removal

from Pt by oxidation to CO<sub>2</sub>, as predicted by another theoretical study.<sup>22</sup> The present study indicated that Pt<sub>2</sub>Ru<sub>3</sub> composition could be a good choice for developing high CO-tolerant anode catalyst in PEFC. In the future, we will extend these studies by using larger molecular systems to investigate and stability of Pt<sub>2</sub>Ru<sub>3</sub> against CO.

#### ACKNOWLEDGMENTS

We are grateful to the New Energy and Industrial Technology Development Organization (NEDO) for providing financial support.

#### REFERENCES

- G. Hoogers and D. Thompsett: Catalysis in proton exchange membrane fuel cell technology. *Cattech* **3**, 106 (2000).
- H.A. Gasteiger, N. Markovic, P.N. Ross, and E.J. Cairns: Co electrooxidation on well-characterized Pt–Ru alloys. *J. Phys. Chem.* **98**, 617 (1994).
- M. Watanabe, H. Igarashi, and T. Fujino: Design of CO tolerant anode catalysts for polymer electrolyte fuel cell. *Electrochemistry* **67**, 1194 (1999).
- G. Avgouropoulos and T. Ioannides: CO tolerance of Pt and Rh catalysts: Effect of CO in the gas-phase oxidation of H<sub>2</sub> over Pt and Rh supported catalysts. *Appl. Catal., B* **56**, 77 (2005).
- K. Wang, H.A. Gasteiger, N.M. Markovic, and P.N. Ross: On the reaction pathway for methanol and carbon monoxide electrooxidation on Pt–Sn alloy versus Pt–Ru alloy surfaces. *Electrochim. Acta* **41**, 2587 (1996).
- L. Carrette, K.A. Friedrich, and U. Stimming: Fuel cells—fundamentals and applications. *Fuel Cells* **1**, 5 (2001).
- R. Ferrando, J. Jellinek, and R.L. Johnston: Nanoalloys: From theory to applications of alloy clusters and nanoparticles. *Chem. Rev.* **108**(3), 845 (2008).
- T. Yajima, H. Uchida, and M. Watanabe: In situ ATR-FTIR spectroscopic study of electro-oxidation of methanol and adsorbed CO at Pt–Ru alloy. *J. Phys. Chem. B* **108**, 2654 (2004).
- W.F. Lin, M.S. Zei, M. Eiswirth, G. Ertl, T. Iwasita, and W. Vielstich: Electro-catalytic activity of Ru-modified Pt(111) electrodes toward CO oxidation. *J. Phys. Chem. B* **103**, 6968 (1999).
- K.-W. Park and Y.-E. Sung: Catalytic activity of platinum on ruthenium electrodes with modified (electro) chemical states. *J. Phys. Chem. B* **109**, 13585 (2005).
- C. Lu, C. Rice, R.I. Masel, P.K. Babu, P. Waszczuk, H.S. Kim, E. Oldfield, and A. Wieckowski: UHV, electrochemical NMR, and electrochemical studies of platinum/ruthenium fuel cell catalysts. *J. Phys. Chem. B* **106**, 9581 (2002).
- F.B. de Mongeot, M. Scherer, B. Gleich, E. Kopatzki, and R.J. Behm: CO adsorption and oxidation on bimetallic Pt/Ru (0001) surfaces—A combined STM and TPD/TPR study. *Surf. Sci.* **411**, 249 (1998).
- Q. Ge, S. Desai, M. Neurock, and K. Kourtakis: CO adsorption on Pt–Ru surface alloys and on the surface of Pt–Ru bulk alloy. *J. Phys. Chem.* **105**, 9533 (2001).
- C. Pistonese, E. Pronzato, and A. Juan: A DFT study of H adsorption on Pt(111) and Pt–Ru(111) surfaces. *Appl. Surf. Sci.* **254**, 5827 (2008).
- H. Orita, N. Itoh, and Y. Inada: All electron scalar relativistic calculations on adsorption of CO on Pt(111) with full-geometry optimization: A correct estimation for CO site-preference. *Chem. Phys. Lett.* **384**, 271 (2004).

16. M.T.M. Koper, T.E. Shubina, and R.A. van Santen: Periodic density functional study of co and OH adsorption on Pt–Ru alloy surfaces: Implications for co tolerant fuel cell catalysts. *J. Phys. Chem. B* **106**, 686 (2002).
17. Y. Shimodaira, T. Tanaka, T. Miura, A. Kudo, and H. Kobayashi: Density functional theory study of anode reactions on Pt-based alloy electrodes. *J. Phys. Chem. C* **111**, 272 (2007).
18. P. Liu, A. Logadottir, and J.K. Nørskov: Modeling the electro-oxidation of co and H<sub>2</sub>/CO on Pt, Ru, PtRu and Pt<sub>3</sub>Sn. *Electrochim. Acta* **48**, 3731 (2003).
19. Z. Ji and J.Q. Li: Density functional study of CO oxidation on Pt and PtMo. *Chem. Phys. Lett.* **424**, 111 (2006).
20. Z. Ji, A.F. Jalbout, and J.Q. Li: Adsorption and diffusion of OH on Mo modified Pt(111) surface: First-principles theory. *Solid State Commun.* **142**, 148 (2007).
21. M.T.M. Koper and R.A. van Santen: Interaction of H, O and OH with metal surfaces. *J. Electroanal. Chem.* **472**, 126 (1999).
22. B.C. Han and G. Ceder: Effect of coadsorption and Ru alloying on the adsorption of CO on Pt. *Phys. Rev. B* **74**, 205418 (2006).
23. T. Sato, K. Kunimatsu, K. Okaya, H. Yano, M. Watanabe, and H. Uchida: In situ ATR-FTIR analysis of the co-tolerance mechanism on Pt<sub>2</sub>Ru<sub>3</sub>/C catalysts prepared by the nanocapsule method. *Energy Environ. Sci.* **4**, 433 (2011).
24. T. Sato, K. Okaya, K. Kunimatsu, H. Yano, M. Watanabe, and H. Uchida: Effect of particle size and composition on co-tolerance at Pt–Ru/C catalysts analyzed by in situ attenuated total reflection FTIR spectroscopy. *ACS Catal.* **2**, 450 (2012).
25. T. Takeguchi, T. Yamanaka, K. Asakura, E.N. Muhamad, K. Uosaki, and W. Ueda: Evidence of nonelectrochemical shift reaction on a CO-tolerant high-entropy state Pt–Ru anode catalyst for reliable and efficient residential fuel cell systems. *J. Am. Chem. Soc.* **134**, 14508 (2012).
26. Y. Ishikawa, M-S. Liao, and C.R. Cabrera: Energetics of H<sub>2</sub>O dissociation and CO<sub>ads</sub> + OH<sub>ads</sub> reaction on a series of Pt–M mixed metal clusters: A relativistic density-functional study. *Surf. Sci.* **513**, 98 (2002).
27. T.E. Shubina and M.T.M. Koper: Quantum-chemical calculations of CO and OH interacting with bimetallic surfaces. *Electrochim. Acta* **47**, 3621 (2002).
28. B. Delley: An all-electron numerical method for solving the local density functional for polyatomic molecules. *J. Chem. Phys.* **92**, 508 (1990).
29. B. Delley: Fast calculation of electrostatics in crystals and large molecules. *J. Phys. Chem.* **100**, 6107 (1996).
30. B. Delley: From molecules to solids with the DMol<sub>3</sub> approach. *J. Chem. Phys.* **113**, 7756 (2000).
31. J.P. Perdew, K. Burke, and M. Ernzerhof: Generalized gradient approximation made simple. *Phys. Rev. Lett.* **77**, 3865 (1996).
32. Y. Ishikawa, J.J. Mateo, D.A. Tryk, and C.R. Cabrera: Direct molecular dynamics and density functional theoretical study of the electrochemical hydrogen oxidation reaction and underpotential deposition of H on Pt(111). *J. Electroanal. Chem.* **607**, 37 (2007).
33. G.E. Gdowski, J.A. Fair, and R.J. Madix: Reactive scattering of small molecules from platinum crystal surfaces: D<sub>2</sub>CO, CH<sub>3</sub>OH, HCOOH, and the nonanomalous kinetics of hydrogen atom recombination. *Surf. Sci.* **127**, 541 (1983).
34. M.K. Alam and H. Takaba: Density functional theory study of OH and CO adsorption on the Pt<sub>2</sub>Ru<sub>3</sub> surface. *ECS Trans.* **64**(3), 689 (2014).
35. S. Volkenning, K. Bedurftig, K. Jacobi, J. Wintterlin, and G. Ertl: Dual-path mechanism for catalytic oxidation of hydrogen on platinum surfaces. *Phys. Rev. Lett.* **83**, 2672 (1999).
36. G.B. Fisher and B.A. Sexton: Identification of an adsorbed hydroxyl species on the Pt(111) Surface. *Phys. Rev. Lett.* **44**, 683 (1980).
37. M.K. Alam and H. Takaba: Stability of Pt–Ru alloy for anode catalyst in PEFC fuel cell: A density functional theory study. *ECS Trans.* **61**(13), 1 (2014).
38. A.V. Ruban, H.L. Skriver, and J.K. Nørskov: Surface segregation energies in transition-metal alloys. *Phys. Rev. B* **59**, 15990 (1999).